Photothermal inactivation of heat-resistant bacteria on nanoporous gold disk arrays

Greggy M. Santos,[1,6] Felipe Ibañez de Santi Ferrara,[2,3,6] Fusheng Zhao,[1] Debora F. Rodrigues,[2,7] and Wei-Chuan Shih[1,4,5,8]

[1]*Department of Electrical and Computer Engineering, University of Houston, Houston, TX, 77204, USA*
[2]*Department of Civil and Environmental Engineering, University of Houston, Houston, TX, 77204, USA*
[3]*CAPES Foundation, Ministry of Education of Brazil, Brasilia – DF 70040-020, Brazil*
[4]*Department of Biomedical Engineering, University of Houston, Houston, TX, 77204, USA*
[5]*Department of Chemistry, University of Houston, Houston, TX, 77204, USA*
[6]*Contributed equally*
[7]*dfrigirodrigues@uh.edu*
[8]*wshih@uh.edu*

Abstract: A rapid photothermal bacterial inactivation technique has been developed by irradiating near-infrared (NIR) light onto bacterial cells (*Escherichia coli*, *Bacillus subtilis*, *Exiguobacterium* sp. AT1B*)* deposited on surfaces coated with a dense, random array of nanoporous gold disks (NPGDs). With the use of cell viability tests and SEM imaging results, the complete inactivation of the pathogenic and heat-resistant bacterial model strains is confirmed within ~25 s of irradiation of the NPGD substrate. In addition to irradiation control experiments to prove the efficacy of the bacterial inactivation, thermographic imaging showed an immediate averaged temperature rise above 200 °C within the irradiation spot of the NPGD substrate. The light-gated photothermal effects on the NPGD substrate offers potential applications for antimicrobial and nanotherapeutic devices due to strong light absorption in the tissue optical window, i.e., the NIR wavelengths, and robust morphological structure that can withstand high instantaneous thermal shocks.

OCIS codes: (250.5403) Plasmonics; (240.6680) Surface plasmons; (350.5340) Photothermal effects; (120.3890) Medical optics instrumentation; (170.1610) Clinical applications.

References and links

1. R. T. Mayon-White, G. Ducel, T. Kereselidze, and E. Tikomirov, "An international survey of the prevalence of hospital-acquired infection," J. Hosp. Infect. **11**(A), 43–48 (1988).
2. R. K. Root, *Clinical Infectious Diseases: A Practical Approach* (Oxford University Press, 1999).
3. A. I. Hidron, J. R. Edwards, J. Patel, T. C. Horan, D. M. Sievert, D. A. Pollock, S. K. Fridkin, N. H. S. N. Team, and P. N. H. S. N. Facilities; National Healthcare Safety Network Team; Participating National Healthcare Safety Network Facilities, "NHSN annual update: antimicrobial-resistant pathogens associated with healthcare-associated infections: annual summary of data reported to the national healthcare safety network at the centers for disease control and prevention, 2006-2007," Infect. Control Hosp. Epidemiol. **29**(11), 996–1011 (2008).
4. S. S. Block, *Disinfection, Sterilization, and Preservation* (Lippincott Williams & Wilkins, 2001).
5. W.-S. Kuo, C.-M. Wu, Z.-S. Yang, S.-Y. Chen, C.-Y. Chen, C.-C. Huang, W.-M. Li, C.-K. Sun, and C.-S. Yeh, "Biocompatible bacteria@Au composites for application in the photothermal destruction of cancer cells," Chem. Commun. (Camb.) **37**, 4430–4432 (2008).
6. X. Huang, I. H. El-Sayed, W. Qian, and M. A. El-Sayed, "Cancer cell imaging and photothermal therapy in the near-infrared region by using gold nanorods," J. Am. Chem. Soc. **128**(6), 2115–2120 (2006).
7. R. S. Norman, J. W. Stone, A. Gole, C. J. Murphy, and T. L. Sabo-Attwood, "Targeted photothermal lysis of the pathogenic bacteria, Pseudomonas aeruginosa, with gold nanorods," Nano Lett. **8**(1), 302–306 (2008).
8. E. S. Tuchina, P. O. Petrov, K. V. Kozina, F. Ratto, S. Centi, R. Pini, and V. V. Tuchin, "Using gold nanorods labelled with antibodies under the photothermal action of NIR laser radiation on Staphylococcus aureus," Quantum Electron. **44**(7), 683–688 (2014).
9. O. Khantamat, C.-H. Li, F. Yu, A. C. Jamison, W.-C. Shih, C. Cai, and T. R. Lee, "Gold nanoshell-decorated silicone surfaces for the Near-Infrared (NIR) photothermal destruction of the pathogenic bacterium e. faecalis," ACS Appl. Mater. Interfaces **7**(7), 3981–3993 (2015).

#256863 Received 8 Jan 2016; revised 26 Feb 2016; accepted 28 Feb 2016; published 17 Mar 2016

10. V. P. Zharov, K. E. Mercer, E. N. Galitovskaya, and M. S. Smeltzer, "Photothermal nanotherapeutics and nanodiagnostics for selective killing of bacteria targeted with gold nanoparticles," Biophys. J. **90**(2), 619–627 (2006).
11. J. P. Houston, A. B. Thompson, M. Gurfinkel, and E. M. Sevick-Muraca, "Sensitivity and depth penetration of continuous wave versus frequency-domain photon migration near-infrared fluorescence contrast-enhanced imaging," Photochem. Photobiol. **77**(4), 420–430 (2003).
12. B. Brooksby, S. Jiang, H. Dehghani, B. W. Pogue, K. D. Paulsen, J. Weaver, C. Kogel, and S. P. Poplack, "Combining near-infrared tomography and magnetic resonance imaging to study in vivo breast tissue: implementation of a Laplacian-type regularization to incorporate magnetic resonance structure," J. Biomed. Opt. **10**, 051504 (2005).
13. W. C. Huang, P. J. Tsai, and Y. C. Chen, "Functional gold nanoparticles as photothermal agents for selective-killing of pathogenic bacteria," Nanomedicine (Lond.) **2**(6), 777–787 (2007).
14. Y. Zhao and X. Jiang, "Multiple strategies to activate gold nanoparticles as antibiotics," Nanoscale **5**(18), 8340–8350 (2013).
15. V. K. Pustovalov, A. S. Smetannikov, and V. P. Zharov, "Photothermal and accompanied phenomena of selective nanophotothermolysis with gold nanoparticles and laser pulses," Laser Phys. Lett. **5**(11), 775–792 (2008).
16. G. M. Santos, F. Zhao, J. Zeng, and W.-C. Shih, "Characterization of nanoporous gold disks for photothermal light harvesting and light-gated molecular release," Nanoscale **6**(11), 5718–5724 (2014).
17. J. Qi, P. Motwani, M. Gheewala, C. Brennan, J. C. Wolfe, and W.-C. Shih, "Surface-enhanced Raman spectroscopy with monolithic nanoporous gold disk substrates," Nanoscale **5**(10), 4105–4109 (2013).
18. G. M. Santos, F. Zhao, J. Zeng, M. Li, and W. C. Shih, "Label-free, zeptomole cancer biomarker detection by surface-enhanced fluorescence on nanoporous gold disk plasmonic nanoparticles," J. Biophotonics **8**(10), 855–863 (2015).
19. M. Li, Y. Du, F. Zhao, J. Zeng, C. Mohan, and W.-C. Shih, "Reagent- and separation-free measurements of urine creatinine concentration using stamping surface enhanced Raman scattering (S-SERS)," Biomed. Opt. Express **6**(3), 849–858 (2015).
20. Y. Zhu, M. Ramasamy, and D. K. Yi, "Antibacterial activity of ordered gold nanorod arrays," ACS Appl. Mater. Interfaces **6**(17), 15078–15085 (2014).
21. S. K. Kim, C.-J. Heo, J. Y. Choi, S. Y. Lee, S. G. Jang, J. Won Shim, T. S. Seo, and S.-M. Yang, "Photothermolysis of immobilized bacteria on gold nanograil arrays," Appl. Phys. Lett. **98**(23), 233701 (2011).
22. M. M. P. Arnob, F. Zhao, J. Zeng, G. M. Santos, M. Li, and W.-C. Shih, "Laser rapid thermal annealing enables tunable plasmonics in nanoporous gold nanoparticles," Nanoscale **6**(21), 12470–12475 (2014).
23. T. A. Vishnivetskaya, S. Lucas, A. Copeland, A. Lapidus, T. Glavina del Rio, E. Dalin, H. Tice, D. C. Bruce, L. A. Goodwin, S. Pitluck, E. Saunders, T. Brettin, C. Detter, C. Han, F. Larimer, M. L. Land, L. J. Hauser, N. C. Kyrpides, G. Ovchinnikova, S. Kathariou, R. F. Ramaley, D. F. Rodrigues, C. Hendrix, P. Richardson, and J. M. Tiedje, "Complete genome sequence of the Thermophilic Bacterium Exiguobacterium sp. AT1b," J. Bacteriol. **193**(11), 2880–2881 (2011).
24. K. D. Pangilinan, C. M. Santos, N. C. Estillore, D. F. Rodrigues, and R. C. Advincula, "Temperature-responsiveness and antimicrobial properties of CNT-PNIPAM hybrid brush films," Macromol. Chem. Phys. **214**(4), 464–469 (2013).
25. E. G. Velliou, E. Van Derlinden, A. M. Cappuyns, A. H. Geeraerd, F. Devlieghere, and J. F. Van Impe, "Heat inactivation of Escherichia coli K12 MG1655: Effect of microbial metabolites and acids in spent medium," J. Therm. Biol. **37**(1), 72–78 (2012).
26. J. L. Edwards, Jr., F. F. Busta, and M. L. Speck, "Thermal inactivation characteristics of bacillus subtilis spores at ultrahigh temperatures," Appl. Microbiol. **13**(6), 851–857 (1965).
27. M. L. Droffner and N. Yamamoto, "Isolation of thermophilic mutants of Bacillus subtilis and Bacillus pumilus and transformation of the thermophilic trait to mesophilic strains," J. Gen. Microbiol. **131**(10), 2789–2794 (1985).
28. F. Zhao, J. Zeng, M. M. Parvez Arnob, P. Sun, J. Qi, P. Motwani, M. Gheewala, C.-H. Li, A. Paterson, U. Strych, B. Raja, R. C. Willson, J. C. Wolfe, T. R. Lee, and W.-C. Shih, "Monolithic NPG nanoparticles with large surface area, tunable plasmonics, and high-density internal hot-spots," Nanoscale **6**(14), 8199–8207 (2014).
29. C. M. Santos, J. Mangadlao, F. Ahmed, A. Leon, R. C. Advincula, and D. F. Rodrigues, "Graphene nanocomposite for biomedical applications: fabrication, antimicrobial and cytotoxic investigations," Nanotechnology **23**(39), 395101 (2012).
30. I. E. Mejías Carpio, C. M. Santos, X. Wei, and D. F. Rodrigues, "Toxicity of a polymer-graphene oxide composite against bacterial planktonic cells, biofilms, and mammalian cells," Nanoscale **4**(15), 4746–4756 (2012).
31. F. Ahmed, C. M. Santos, J. Mangadlao, R. Advincula, and D. F. Rodrigues, "Antimicrobial PVK:SWNT nanocomposite coated membrane for water purification: performance and toxicity testing," Water Res. **47**(12), 3966–3975 (2013).
32. W.-C. Shih, K. Bechtel, and M. S. Feld, "Noninvasive glucose sensing with Raman spectroscopy," in *Analytical Chemistry of In Vivo Glucose Measurements* (John Wiley & Sons, 2009), pp. 391–419.

#256863 Received 8 Jan 2016; revised 26 Feb 2016; accepted 28 Feb 2016; published 17 Mar 2016

33. J. Zeng, F. Zhao, J. Qi, Y. Li, C.-H. Li, Y. Yao, T. R. Lee, and W.-C. Shih, "Internal and external morphology-dependent plasmonic resonance in monolithic nanoporous gold nanoparticles," RSC Advances **4**(69), 36682–36688 (2014).
34. J. Zeng, F. Zhao, M. Li, C.-H. Li, T. R. Lee, and W.-C. Shih, "Morphological control and plasmonic tuning of nanoporous gold disks by surface modifications," J. Mater. Chem. C Mater. Opt. Electron. Devices **3**(2), 247–252 (2015).
35. Z. Fan, D. Senapati, S. A. Khan, A. K. Singh, A. Hamme, B. Yust, D. Sardar, and P. C. Ray, "Popcorn-shaped magnetic core-plasmonic shell multifunctional nanoparticles for the targeted magnetic separation and enrichment, label-free SERS imaging, and photothermal destruction of multidrug-resistant bacteria," Chemistry **19**(8), 2839–2847 (2013).
36. T. Miyamoto, S. Okano, and N. Kasai, "Inactivation of Escherichia coli endotoxin by soft hydrothermal processing," Appl. Environ. Microbiol. **75**(15), 5058–5063 (2009).
37. B. M. Mackey, C. A. Miles, S. E. Parsons, and D. A. Seymour, "Thermal denaturation of whole cells and cell components of Escherichia coli examined by differential scanning calorimetry," J. Gen. Microbiol. **137**(10), 2361–2374 (1991).
38. W.-C. Shih, C. W. Wong, Y. B. Jeon, S.-G. Kim, and G. Barbastathis, "MEMS tunable gratings with analog actuation," Inf. Sci. **149**(1-3), 31–40 (2003).

1. Introduction

The risks of contracting a hospital-acquired (nosocomial) infection has long been a real threat and the rate can be as high as 13.5% in certain countries [1, 2]. Among the major causes of high risks of bacterial infection are the type of patient's disease, surgical procedures, and urinary tract infections [3]. The most important trait of a disease-causing bacterium, responsible for the nosocomial infections, is its antibiotic resistance. This adaptation allows the bacteria to survive treatment with antibiotics and, frequently, results in fatal diseases to patients [3]. Considering pathogenic bacteria continuously evolve to be resistant to an increasing number of commercial antibiotics, it is essential to develop reliable and effective methods to inactivate bacterial viability and proliferation. Exposure to high temperatures is a well-known method for this purpose, commonly used to disinfect laboratory tools and medical instrumentation using standard sterilization equipment such as dry ovens or autoclaves. These methods are effective, however, they require long sterilization durations (several minutes to hours) [4]. To overcome this limitation, a simple coating of various gold nanoparticles have been pursued as an alternative approach with the potential for *in situ* sterilization.

Due to its effective light absorption, gold nanoparticles had been extensively studied to generate photothermal heat for therapeutic applications such as cancer therapy [5, 6] and the inactivation of harmful bacterial activity [7–10]. The particular advantages of certain gold nanoparticles (i.e. nanoshells, nanorods) are its near-infrared (NIR) plasmonic resonance. NIR light as an excitation sources is relatively safe for body tissues at controlled power conditions with excellent penetration depth for biological tissue, which makes it a good choice for localized heating for *in situ* applications [11, 12]. Photothermal conversion of absorbed NIR light results in an overall temperature increase to the surrounding medium of low thermal conductivity. Gold nanoparticles were shown to induce thermal inactivation of different types of bacteria such as *Escherichia coli*, *Pseudomonas aeruginosa, Staphylococcus aureus* and *Bacillus subtilis* [7, 13, 14]. In the majority of these studies, heat damage to the bacterial cell wall was the primary cause of cell death [15]. Once the cell wall is damaged, many essential functions such as substance transport, ATP synthesis, and other cell maintenance processes are significantly compromised.

We recently characterized the photothermal properties of newly developed nanoporous gold disks (NPGDs) and its ability to promote light-gated multi-stage molecular release [16]. Upon the excitation with incident light, localized surface plasmon resonance (LSPR) of the NPGD nanoparticles enhances the local electric field within its nanoporous networks. The LSPR results in radiative and non-radiative decay mechanisms that have been utilized for several applications such as Raman and fluorescence enhancement, biomolecular sensing, and NIR-gated photothermal processes [16–19]. Being tailored to strongly absorb NIR light, irradiated NPGDs were shown to induce nearly instantaneous temperature increase from the

#256863 Received 8 Jan 2016; revised 26 Feb 2016; accepted 28 Feb 2016; published 17 Mar 2016

irradiated spot and across the random array substrate, delivering thermal shocks into the surrounding medium [16]. With sufficient heat generated from the NPGD arrays towards the bacteria, real-time inactivation within a few seconds of irradiation can be achieved, considerably shorter than on nanoparticle arrays demonstrated in recent studies [9, 10, 20, 21]. Another advantage of NPGD arrays as a reliable light-gated photothermal substrate for direct bacterial inactivation is that it does not require additional surface modifications for preventing particle aggregation in solution typical in dispersed nanoparticles. Moreover, using the optimal irradiation conditions, the nanoparticles maintain a consistently high photothermal conversion efficiency without morphological changes in its nanostructure [16, 22]. In other words, NPGD arrays can undergo multiple photothermal cycles without the loss of efficiency, a critical feature for preventing recurring bacterial proliferation *in situ*. The NPGD array can also be employed as a fixed antibacterial substrate for disinfecting contaminated liquid flow systems. Hence, these characteristics of the NPGD random array make it a robust and rapid antibacterial platform suitable for various biomedical applications.

A vast majority of the nosocomial infections are caused by either Gram-positive (Gram +) or Gram-negative (Gram -) bacteria [3]. The bacteria used in this study are: *Escherichia coli* MG 1655 (Gram -) and *Bacillus subtilis* 102 (Gram +), and a thermophilic *Exiguobacterium sp.* strain AT1b *(Gram +)* [23, 24]. The rationale for the selection of these microorganisms was to use different groups of bacteria with different cell wall structures and heat resistance to investigate the effectiveness of the photothermal inactivation method using NPGD random arrays. In this study, *E. coli* MG 1655 was selected because it is a surrogate for other pathogenic *E. coli* strains that can be inactivated at temperatures *<60 °C* [25]. *B. subtilis* is able to survive temperatures over 50 °C and *Exiguobacterium* sp. AT1b can grow in temperatures of up to 55 °C [23, 26, 27]. With the diversity of thermal tolerance of these bacterial samples, the versatility range of the thermal inactivation method using the NPGD array is evaluated for its applicability for other potentially pathogenic and heat-resistant bacterial species. In this study, the destructive effects of the photothermal bacterial inactivation on NPGD array are reported using cell viability tests, thermographic imaging and scanning-electron microscopy (SEM). In relation to previous studies on inactivation methods using nanoparticle arrays, our results show the strong potential of NPGDs for instantaneous (~seconds) disinfection of nosocomial bacteria *in situ*.

2. Experimental section

2.1 Nanoporous gold disk fabrication

NPG disks (400 nm in diameter, 75 nm thickness, and 13 nm average pore size) were fabricated according to methods in recent published studies [17, 28]. The fabrication of substrate-bound NPGD arrays initiates with DC sputtering of a 120 nm thick film of Au: Ag (30: 70) alloy over the glass coverslip (~165 μm thick). A monolayer of 600 nm polystyrene (PS) beads was then deposited on the surface of the alloy film. To shrink and isolate the PS beads, oxygen plasma-etching was employed, followed by Ar plasma-etching to induce alloy disk formation on the glass surface. The remaining PS beads on top of the alloy disks were removed by dissolution in chloroform. The disks were dealloyed in 70% nitric acid for 1 min, followed by DI water wash for 2 min. This nanoparticle array on the glass coverslip is referred to as the "NPGD substrate" in the subsequent text.

2.2 Bacterial growth conditions

The bacterial strains used in the present study were *E. coli* MG 1655, *B. subtilis* 102 and *Exiguobacterium* sp. AT1b [23, 24, 29]. For all three microorganisms, tryptic soy broth (TSB) was used as the growth media (Oxoid Ltd., Hampshire, England). Phosphate-buffered saline tablets (0.01 M, pH = 7.4 at 25 °C, 0.0027 KCl, 0.137 NaCl, Fisher Scientific, USA) were used to prepare the bacterial phosphate buffer saline solution (PBS) [30]. An isolated bacterial

#256863 Received 8 Jan 2016; revised 26 Feb 2016; accepted 28 Feb 2016; published 17 Mar 2016

colony was grown in 5 mL of TSB overnight at 35 °C. After which, the bacterial culture was centrifuged at 10000 g for 10 min, and the bacterial pellet was washed once and resuspended in PBS buffer. The optical density (OD) of the resulting suspension was adjusted to 0.50 at 600 nm, which corresponds to a concentration of about 10^6 to 10^7 colony forming units per milliliter (CFU/mL).

2.3 Scanning electron microscopy (SEM)

SEM images of the fabrication process of the NPGD substrate can be found in recent papers published [17, 28]. Top and oblique SEM views of the NPGD nanoparticle arrays are shown in Fig. 1. To resolve the bacterial cells on the NPGD substrate using SEM, the bacteria-NPGD samples were prepared using a bacterial fixation procedure previously described [31]. Briefly, the bacteria-NPGD samples were fixed using 2% glutaraldehyde solution in 0.05 M sodium cacodylate buffer. The samples were incubated for 30 min at room temperature and then for 60 min at 4 °C with 300 µL of the glutaraldehyde-cacodylate buffer. The samples were washed by incubating for 10 min with 300 µL of 0.05 M sodium cacodylate buffer for three times. Then, the cells were incubated with 1% osmium tetraoxide for 30 min. The samples were then washed three times with 0.05 M cacodylate buffer as previously described. Dehydration was performed by placing 300 µL of ethanol of incremental concentrations (25, 50, 75, 95 and 100% v/v) for 15 min before draining and adding the next ethanol solution. After treating with 100% ethanol, the samples were immersed in propylene oxide (100%) for 15 min. The samples were sputter-coated with a 50 nm thick Au film. The samples were then analyzed with a field emission gun scanning electron microscope (FEI XL-30 FEG SEM, Philips).

2.4 NIR exposure and thermal imaging

The 785 nm laser source was generated from a continuous-wave (cw) Titanium:sapphire laser (Spectra-Physics 3900S) pumped by a diode-pumped solid-state 532 nm laser (Spectra-Physics Millennia X). Thermal maps were acquired from irradiated samples using an infrared thermographic camera (A320G, FLIR) recording 16 bit 320 × 240 pixel images at 60 Hz acquisition frame rate (16 ms temporal resolution limit). The camera has an uncooled focal plane array microbolometer with a spectral range of 7.5 to 13 µm and a temperature sensitivity of 50 millikelvins. Temporal plots of local temperature on the irradiated spot of the sample were recovered from thermal imaging videos using FLIR ResearchIR software.

2.5 Bacterial cell irradiation

For each bacterial sample, four pieces of glass coverslips (~16 mm^2) were prepared and two of them were coated with NPGDs. The glass coverslips were attached to the bottom of the well of single cavity glass slides using a two-sided adhesive tape. A 50 µL drop of the bacterial suspension in PBS was placed on each of the four coverslips and incubated for 45 min. The samples were subsequently covered with another glass coverslip, to keep the PBS solution from evaporating during the irradiation process. The coverslips were then irradiated (thermal run) with a 3-mm 785 nm laser spot (600 mW) for 5, 10, 15, 20, 25 and 30 s. The laser spot size was measured using optical images of the beam profile on a CMOS camera with calculations based on the $1/e^2$ approximation. Aside from the thermal run, three separate control experiments were performed for each bacterial strain. One glass coverslip without NPGDs was not irradiated to test the life expectancy of the bacterial strains inside the covered glass slides (control 1). Another coverslip with NPGDs was not irradiated to test its toxicity to the bacterial strains (control 2). Lastly, one coverslip without NPGDs was irradiated to test the effect of irradiation on cell viability (control 3). The schematic in Fig. 2 provides an overview of the thermal run and control experiments. The samples for the thermal and control experiments were equilibrated for 20 min before the irradiation and cell viability measurements.

#256863 Received 8 Jan 2016; revised 26 Feb 2016; accepted 28 Feb 2016; published 17 Mar 2016

2.6 Cell viability assay

After the irradiation procedure, the bacteria were immediately stained for cell viability assays. The total amount of live and dead cells in the bacteria–NPGD substrate was determined using the Live/Dead Baclight bacterial viability staining kit (Invitrogen). A 10:1 mixture of SYTO9 nucleic acid stain and propidium iodide (PI) were added to the solution on each slide. The slides were observed and the images were taken in a BX-51 Olympus fluorescent microscope equipped with a DP72 digital color camera and a 40x objective lens. The fluorescence was acquired using dual band excitation and emission filter sets for fluorescein isothiocyanate (FITC) and tetramethylrhodamine isothiocyanate (TRITC). Using Cell Sens Dimension digital imaging software (Olympus), the percentage of inactive cells from each image was determined and expressed as the percent of the ratio of the total number of inactive (red) cells to the total number of bacteria (green) with a field of view (FOV) of 800 μm^2 (100 μm x 80 μm).

3. Results and discussion

First, we investigate the physical nanostructural features of the NPGD substrate to define its suitability as a plasmonic heat source material. The NPG disks (400 nm in diameter, 75 nm thickness, and 13 nm average pore size) were fabricated according to methods recently published (see Experimental Section) [17]. The SEM images show the surface morphology and monolayer distribution of the patterned NPGDs on the glass coverslip (Figs. 1(a) and 1(b)). The 90° oblique-view SEM images indicate uniform thickness (~75 nm) of the NPGDs with an average diameter of 400 nm (Figs. 1(c) and 1(d)). With a monolayer coverage of ~50%, the NPGD nanoparticles are separated in between by the bare glass surface. The uniform thickness and monolayer coverage of the NPGDs on the glass surface ensures homogeneous heat transfer from the patterned nanostructure to the adjacent environment. Moreover, the transmission extinction spectra of the NPGD substrate is shown in Fig. 1(e) where the absorption maximum is at 1050 nm. In a previous study, we determined the photothermal conversion efficiency for the NPGD substrate at 56% at the NIR wavelengths (700-900 nm) [16]. Aside from the high penetration depth of NIR light for biological material (tissue and bacteria), the laser wavelength used (785 nm) provides sufficient photothermal conversion resulting to heat transfer to surrounding media due to the effective absorption of NPGD array at this broad NIR wavelength range. Nevertheless, deeper tissue penetration can be potentially achieved with similar photothermal efficiency using wavelengths ~1000-1200 nm [32].

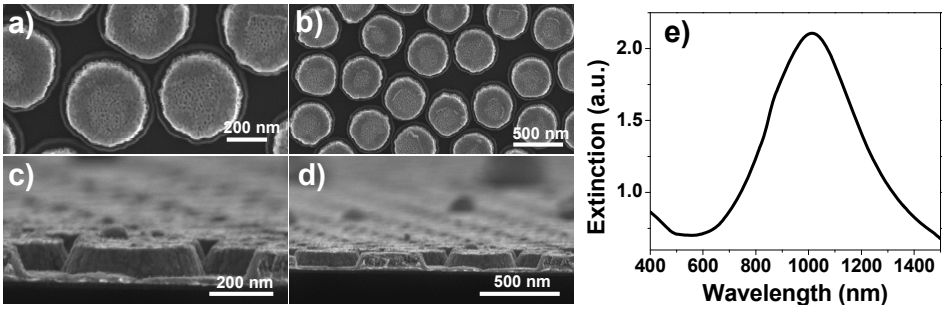

Fig. 1. Scanning electron microscopy (SEM) images of nanoporous gold disks (NPGDs) arrays on glass at different magnifications: (a,c) 200,000x (scale bar ~200 nm) and (b,d) 100,000x (scale bar ~500 nm) at top and oblique (90°) views, respectively. (e) Normalized extinction spectra of NPGDs (disk diameter: 400 nm).

#256863 Received 8 Jan 2016; revised 26 Feb 2016; accepted 28 Feb 2016; published 17 Mar 2016

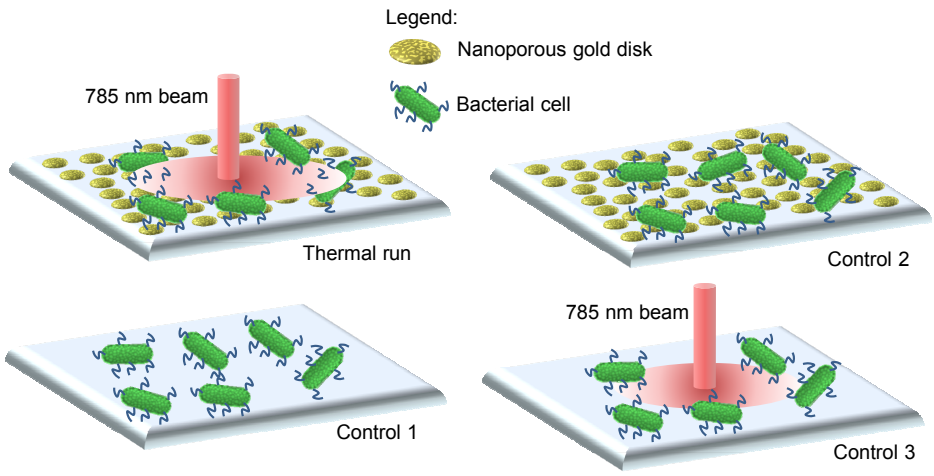

Fig. 2. Schematic diagram of the thermal run and control experiments. Control 1: A non-irradiated glass substrate was used to test the life expectancy of the bacterial strains inside the covered glass slides. Control 2: A non-irradiated NPGD substrate was tested for its toxicity to the bacterial samples. Control 3: One coverslip without NPGD was irradiated to test the effect of irradiation on cell viability.

With the use of a thermal imaging camera, the heat propagation from the region directly irradiated by the NIR beam is visualized as a temperature distribution map across the NGPD sample. The NIR irradiation of the bare NPGD substrate (exposure time: 30 s) generated local maximum temperatures (T_{max}) above 200 °C on the nanomaterial surface (Figs. 3(a)-3(c)). To evaluate the heat transfer from the irradiated NPGD substrate to the surrounding media, 50 µL of PBS buffer solution (same volume of bacterial solution used in the irradiation experiments) was sandwiched between the NPGD substrate and the glass coverslip. The thermal measurements were collected from the glass coverslip placed on top of the wet NPGD substrate. A T_{max} of ~100 °C was recovered from the irradiated portion of the sample (Fig. 3(d)). We note that the actual local temperature on the NPGD surface is expected to be higher compared to the local temperature measurement. The lower temperature of the glass coverslip on top of the wet NPGD substrate resulted from the heat diffusion from the nanostructure to the surrounding materials: PBS aqueous solution, glass and air. From Fig. 3(b), the temperature elevation rate for the first 3 s of irradiation is 26 and 67 °C/s for the sandwich (NPGD/water/glass/air) configuration and the bare NPGD surface, respectively. The initial rate for the bare NPGD demonstrate the average temperature elevation from the irradiated spot of the substrate. The difference in the initial rate of the two experiments can be correlated to heat transfer rate from the NPGD surface to the surrounding medium. The average temperature elevation in the aqueous solution can be estimated from these initial rates (~50 °C/s), suggesting that a temperature of more than 100 °C after 3 s of irradiation can be reached in the aqueous layer where the bacterial cells are immersed. The LSPR-tunability of the NPGD material in the NIR range permitted optimized photothermal conversion resulting to efficient localized heating propagating from the irradiated region [16, 33, 34]. Within a few seconds (<20 s), a local temperature maximum of ~95 °C is achieved with bacteria physically attached on the NPGD surface (Fig. 3(e)). Again, we note that the temperature at the NPGD surface is expected to be higher than on the glass surface where the temperature measurements are taken. Thus, the required temperature conditions (>100 °C) to effectively inactivate the bacterial population through cell wall damage and protein denaturation are achieved upon irradiation in the presence of the bacterial cells on the NPGD substrate.

#256863 Received 8 Jan 2016; revised 26 Feb 2016; accepted 28 Feb 2016; published 17 Mar 2016

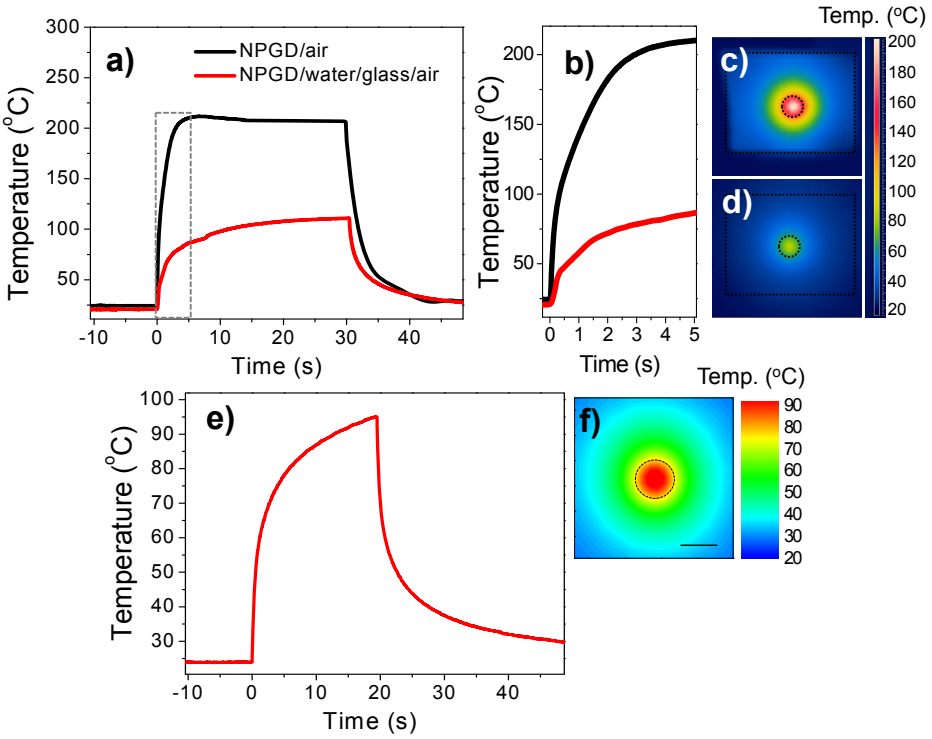

Fig. 3. Thermal imaging measurements of the NPGD substrate. (a) Temporal temperature profile of the irradiated portion of the NPGD substrate with (b) zoomed-in portion (dotted rectangular area) for the temperature rise portion demonstrating thermal transfer rate from NPGD to the water/glass interface. Thermographic image of the temperature distribution of (c) bare NPGD substrate (black curve) and (d) the NPGD substrate with PBS buffer solution sandwiched with another blank glass coverslip at 30 s of irradiation exposure. Using the same irradiation conditions, these samples were exposed without the bacteria present on the NPGD surface. The dotted circle represents the irradiated spot (diameter: 3 mm) on the sample while dotted square represents the area on the glass containing the NPGD array. (e) Temporal temperature profile within the irradiated spot and (f) thermal image of the glass surface on top of the NPGD substrate with *E. coli* bacteria deposited on the surface after 20 s of irradiation exposure. Dotted circle represents the irradiated portion of the NPGD substrate. Scale bar is 3 mm.

In order to validate the antimicrobial properties of the NPGD irradiation on living bacteria, the cell viability assay (see Experimental Section) was performed on irradiated NPGD samples with bacterial cells deposited directly on the nanostructure surfaces. In this task, we investigated the NIR irradiation time required to inactive three different bacterial strains. For the samples at t = 0 s, the cell inactivation was determined immediately upon addition of live cells to the NPGD substrate. After 25 s of exposure, the heat generated was able to inactivate 100% of all bacterial cells investigated (Fig. 4). *E. coli*, as expected, was most vulnerable to the treatment, with 100% inactivation at 5 s of irradiation. *B. subtilis* and *Exiguobacterium* sp. required 25 s to obtain 100% cell inactivation. These results show that this potential sterilization method is efficiently fast compared to the traditional methods (i.e. use of steam-autoclaves and dry-heat ovens) that take about several minutes to hours [4]. Previous studies using power densities in the range of 0.01-0.10 W/mm^2 show that bacterial inactivation on gold nanostructure arrays required longer irradiation times (1-10 min) [9, 10, 20, 21]. In our study, we used a power density of ~0.085 W/mm^2, which allowed us to inactivate all three types of bacteria cells after 25 s of NIR irradiation on the NPGD substrate. The calculated optical energy to inactivate 50% of the bacterial cells (threshold energy) varies

#256863 Received 8 Jan 2016; revised 26 Feb 2016; accepted 28 Feb 2016; published 17 Mar 2016

for each bacterial type. Based on the time-dependence of inactivation in Fig. 3, the *Exiguobacterium* sp. required the most optical energy for all three bacterial types. Taking into account the photothermal conversion efficiency, bacterial density and disk coverage of the substrate, the threshold optical energy estimated for *E. coli*, *B. subtilis* and *Exiguobacterium* sp. are 6, 18 and 30 mJ/mm^2, respectively. The power density required to induce morphological changes is 0.125 W/mm^2 as published in a previous study regarding annealing of NPG disks. At the exposure time and power density conditions used in the study, the NPG disks maintain its morphological features under the irradiation steps used for inactivation [22]. Hence, these results suggest that the irradiation power used on NPGD substrates can be specifically adjusted to further reduce the exposure time, shorter than any photothermal inactivation method on nanoparticle arrays recently reported [9, 20, 21, 35]. Moreover, at the power densities used in the experiment, the NPGD substrate can be subjected to multiple irradiation procedures since it can withstand high instantaneous temperature increase without morphological changes [22]. The preservation of photothermal efficiency of NPGDs after repeated exposures is an essential property for disinfection applications that requires continuous inactivation of recurring bacterial proliferation *in situ*. The efficacy of the method can be further improved by employing NPGD with LSPR peak aligned with the irradiation wavelength. For example, we showed that a higher temperature rise can be obtained at 900 nm, which is closer to the LSPR peak at 1100 nm [16].

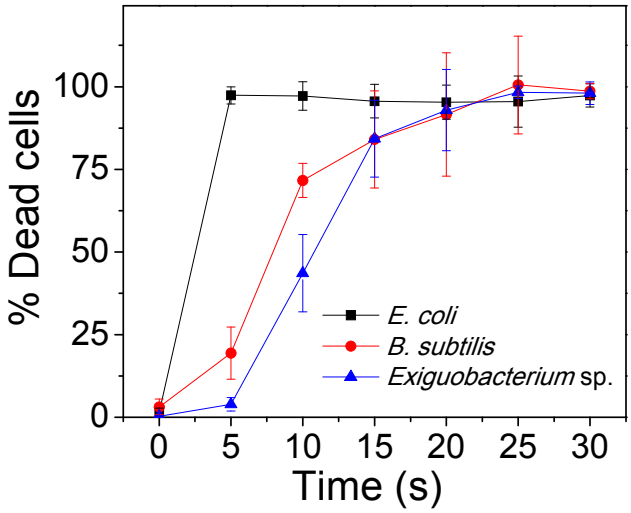

Fig. 4. Percentage of dead cells of *E. coli* MG 1655, *B. subtilis* 102 and *Exiguobacterium* sp. AT1b on NPGD substrate when exposed to laser (785 nm, 0.085 W/mm2) for 0 to 30 s.

Based on the time-dependent cell viability in Fig. 4, the irradiation of NPGD for 25 s resulted in total inactivation of the three bacterial strains. To investigate whether the light-triggered localized temperature elevation from the NPGD substrates were the cause of the bacterial inactivation, control experiments were performed. An overview of the experiments is provided in the schematic in Fig. 2. The first control experiment provides a baseline count of dead cells in the bacterial population. This control involved adding the suspension of bacterial cells to a bare glass slide without exposure to NIR irradiation. As expected, the number of dead cells were minimal since the samples were prepared with freshly grown bacterial cultures (Fig. 5). Any of the consequent bacterial death is a result of the characteristic life expectancy of the microorganisms in PBS buffer inside the glass slides during the experimental procedure.

#256863 Received 8 Jan 2016; revised 26 Feb 2016; accepted 28 Feb 2016; published 17 Mar 2016

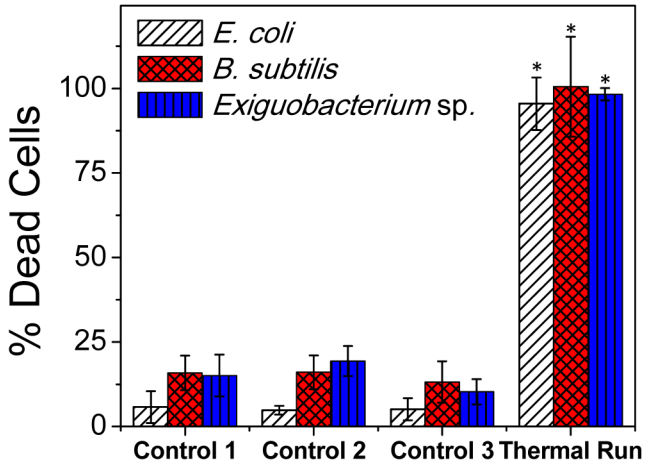

Fig. 5. Cell death counts (at time: 25 s) for the bacterial strains: *E. coli* MG 1655, *B. subtilis* 102 and *Exiguobacterium* sp. AT1b. Three separate control experiments were performed for each bacterial strain. *Statistical significant difference between the thermal run and the controls was tested by one-way ANOVA and Tukey test ($p<0.001$). Refer to Fig. 2 for specific experimental configurations.

The second control experiment involved the NPGD substrate with live bacterial deposits that was not irradiated with the NIR source. This control aimed to determine whether NPGD substrates had inherent antimicrobial properties. The results showed that the cell viability was insignificantly affected by the NPGD substrate as seen from the small numbers of red-stained cells observed (Fig. 6 and Fig. 8, Appendix).

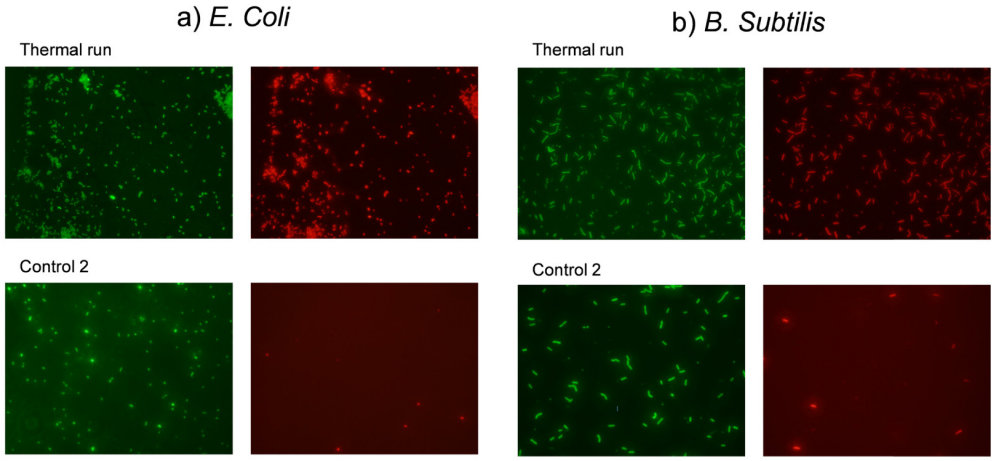

Fig. 6. Total (green) and dead (red) cell count images of (a) *E. coli* K-12 and (b) *B. subtilis* cells on the surfaces of NPGDs showing viability dependence on NIR irradiation. Thermal run: bacteria cells on NPGD exposed to NIR for 25 s; Control 2: bacteria cells on NPGD without NIR exposure. The field-of-view of the image covers an area of 800 μm^2 (100 µm x 80 µm) of the sample.

The third control experiment aimed to investigate the effect of the NIR irradiation to the bacterial cells. In this control, a bare glass slide with bacteria deposited on top was irradiated with NIR light for 25 s (based on the complete inactivation of the three bacterial samples with NPGD) before the viability of the cells was determined. The results showed that the NIR irradiation, when applied alone, had statistically insignificant effect in cell viability. The *Exiguobacterium* sp. viability assay images (Fig. 8, in Appendix) for the three control

#256863 Received 8 Jan 2016; revised 26 Feb 2016; accepted 28 Feb 2016; published 17 Mar 2016

experiments suggest negligible bacterial cell death as compared to the thermal run. For the different bacterial strains tested, the controls did not show statistical difference when compared to each other. The one-way ANOVA and Tukey tests were applied to compare the controls of each bacteria and the thermal run of the same bacteria. Controls and thermal runs of different bacteria were not compared to each other. For the three bacterial strains, the ANOVA p values were lower than 0.001 indicating statistical significant differences between the samples. The controls did not present statistical significant differences when compared to each other in any case ($p>0.05$). The thermal runs presented statistical difference to the controls in all tested bacteria ($p<0.01$). These results indicated that the contact with the NPGD and the exposure to the NIR source are not sufficiently harmful to inactivate the microorganisms when applied separately. Therefore, the bacterial inactivation is mainly due to the photothermal effects of the NPGD upon NIR irradiation.

Here, we determine whether the irradiated bacteria on NPGD at 25 s experienced cell structural changes as a result of thermal inactivation. The SEM images of non-irradiated and irradiated cells on the NPGD substrate are shown in Fig. 7. Humid heat is known to induce protein denaturation, making it more effective in cell inactivation when compared to dry heat where cells are inactivated mostly by oxidation of cell material [36]. Thus, keeping the moisture in the system ensures that the process of sterilization of the surface would be faster and more efficient. The protein denaturation of cell structures of *E. coli*, including the cell wall components, can be completely achieved at 95 °C [37]. This phenomenon can be observed in the irradiated *E. coli* sample (Figs. 7(b) and 7(c)) where its cell walls are wrinkled and ruptured compared to those before irradiation in Fig. 7(a). For the irradiated samples of *B. subtilis* (Figs. 7(e) and 7(f)), the outline of the cell wall is observable but appeared more shrunken and hollow compared to the non-irradiated cell in Fig. 7(d). The thermophilic *Exiguobacterium* sp. AT1b exhibited evident structural damage (Figs. 7(h) and 7(i)) where the bacterial cell wall outline is barely noticeable for the irradiated cells. From these SEM images gathered from the irradiated bacterial samples, the bacterial cell wall damage can be attributed to thermal disruption from the nanoparticle array. The laser spot size used accommodates a large surface dimension for heating multiple disks (3×10^7) at a single irradiation step. Based on the SEM images in Fig. 7, the number of disks in contact with each cell for the three bacterial types varies at 5-15 disks per cell. The average threshold optical energy per cell unit can be estimated based on the time-dependent viability results in Fig. 4. For *E. coli*, *B. subtilis* and *Exiguobacterium* sp., the calculated threshold optical energy per bacteria cell is estimated at 10.5, 45.0 and 52.5 nJ, respectively. The *Exiguobacterium* sp. bacterium requires the most optical energy per cell followed closely by *B. subtilis,* showing their higher thermal energy tolerance compared to *E. coli*.

Although the latter two microbes (*B. subtilis* and *Exiguobacterium* sp. AT1b) are known to have good thermal resistance and well-suited to resist harsh conditions, the temperatures achieved were enough to induce substantial cell wall breakage leading to effective cell death. These results demonstrate the applicability of the photothermal inactivation for a range of bacterial species with varied thermal resistance.

#256863 Received 8 Jan 2016; revised 26 Feb 2016; accepted 28 Feb 2016; published 17 Mar 2016

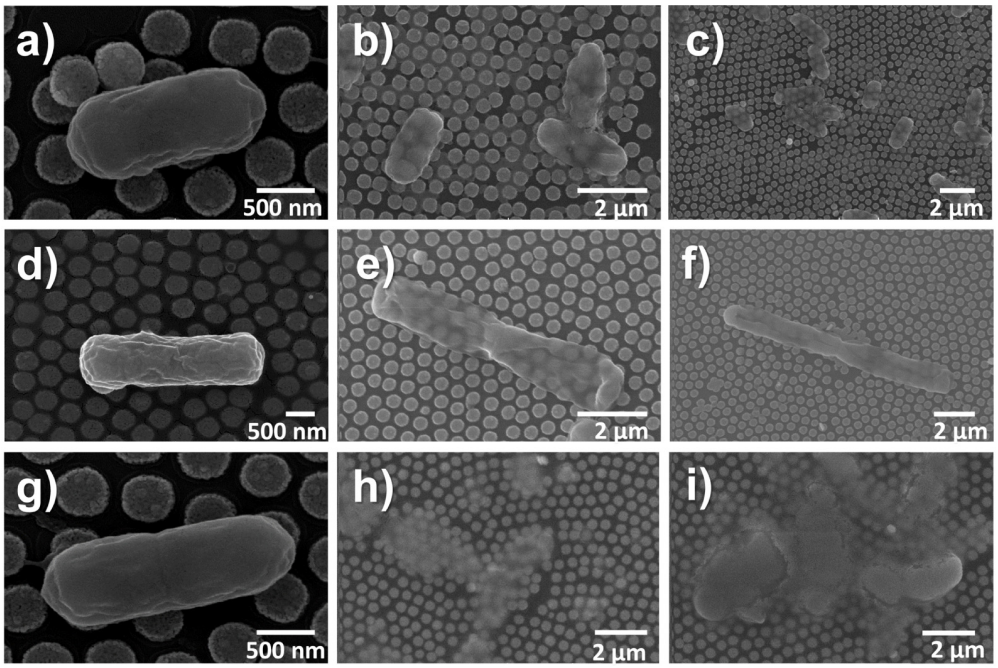

Fig. 7. SEM images of *E. coli* (a, b and c), *B. subtilis* (d, e and f) and *Exiguobacterium* sp. AT1b (g, h and i) cells deposited on the NPGD substrate. The bacteria in the images A, D and G were not exposed to the NIR source. Cells captured in the images b, c, e, f, h and i were exposed to the NIR source on the NPGD substrate for 25 s.

The efficiency in inactivating a wide range of bacterial species (pathogenic, heat resistant and thermophilic) makes the NPGD substrate a potential photothermal plasmonic platform for antibacterial applications. Due to the uniform surface distribution of NPGDs in a random array, the localized heat propagation from the irradiated spot ensures a controlled number of multiple thermal contacts to the adhered bacterial cells [16, 22]. In addition, high-density plasmonic hot spots on NPGD surface play the role of distributed nano-heaters. Together, the NPGD substrate would provide a new micro-actuation mechanism [38]. Since the heat transfer from the nanoparticle array to the surrounding medium are directly affected by the physical properties of the NPGD substrate (i.e. array density, disk diameter and thickness, pore size etc.), modifications in the NPGD fabrication can be employed to match heat transfer requirements to specifically inactivate various bacterial species with specific thermal-resistance characteristics. More importantly, by tailoring the nanoparticle dimensions to optimize absorption of tissue-penetrating NIR light [16, 28], the photothermal conversion of the NPGD substrate can be enhanced further to provide bacterial inactivation for *in vivo* applications. The NPGD nanoparticles absorb strongly in the NIR region that allows permeability for both surface and internal tissue photothermal-mediated bacterial inactivation [16, 28]. Furthermore, compared to methods using dispersed nanoparticle solutions, the robust 2-dimensional nanoparticle arrangement of NPGD arrays make it suitable for expedient isolation from bacterial samples, to allow multiple irradiations cycles on the same substrate. Lastly, we showed in a previous study that, through its large surface area for molecular coverage, the nanoporous network of NPGDs can act as a high capacity molecular payload that can be later released through photothermal mechanisms [16]. The NPGD nanoparticles can be suitably loaded with molecular therapeutic agents to provide added antimicrobial effects. Photothermal inactivation of bacterial population using NPGD substrates provides flexibility for heat generation requirements (broad temperature elevation range, instantaneous

#256863 Received 8 Jan 2016; revised 26 Feb 2016; accepted 28 Feb 2016; published 17 Mar 2016

temperature increase, short sterilization time) to specifically address cell inactivation of diverse sets of bacterial populations.

4. Conclusion

In summary, the NPGD substrate was tested *in vitro* to induce efficient bacterial inactivation using the photothermal effect within a short period of time. With 25 s of NIR illumination, all three bacterial types (*Escherichia coli*, *Bacillus subtilis*, *Exiguobacterium* sp. AT1B*)* were photothermally destroyed by causing irreparable cellular damage, demonstrating the speed and efficiency of NPGD substrate for inactivation of both pathogenic and heat-resistant bacteria. In addition to our initial attempt to control pathogenic bacterial population using the NPGD substrate, nanostructural modifications can further improve its photothermal properties for bacterial inactivation. By fine-tuning the light irradiation properties (power, wavelength, scanning area) and maximizing NIR light absorption of NPGD substrate through nanofabrication techniques, the heat generated can be enhanced to penetrate biological tissues suffering from bacterial infections [10]. The NPGD substrate can potentially serve as a plasmonic microdevice for rapid *in vivo* bacterial inactivation with an advantage of a light-gated mechanism for heat release.

Appendix

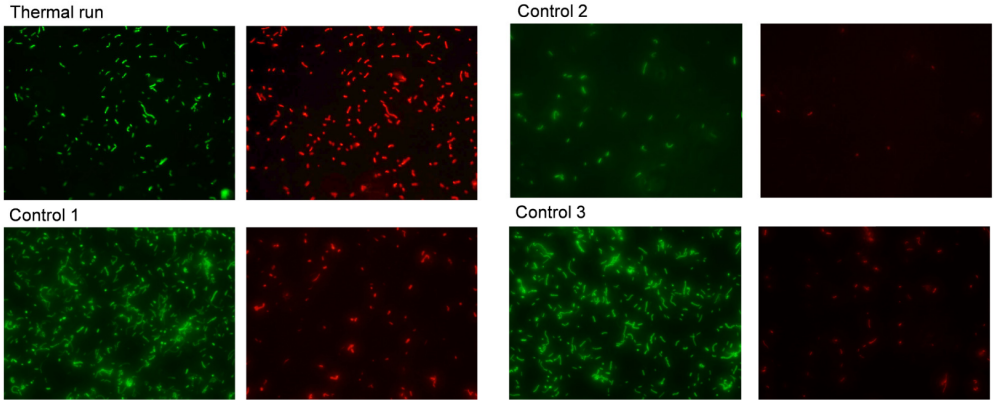

Fig. 8. Total (green) and dead (red) cell count images of *Exiguobacterium* AT1b cells attached NPGDs after exposure to NIR light.; Thermal Run: cells on NPGD exposed to NIR for 25 s; Control 1: control cells on glass without NIR exposure; Control 2: control cells on NPGD without NIR exposure; Control 3: control cells on glass exposed to NIR for 25 s. The field-of-view of the image covers an area of 800 µm2 (100 µm x 80 µm) of the sample.

Acknowledgments

Funding from the National Science Foundation (NSF) CAREER Award (CBET-1151154), the National Aeronautics and Space Administration (NASA) Early Career Faculty Grant (NNX12AQ44G), and the Gulf of Mexico Research Initiative (GoMRI-030) is greatly appreciated.

#256863 Received 8 Jan 2016; revised 26 Feb 2016; accepted 28 Feb 2016; published 17 Mar 2016